Behavioral/Systems/Cognitive

The Chemokine CCL2 Increases $Na_v1.8$ Sodium Channel Activity in Primary Sensory Neurons through a $G\beta\gamma$-Dependent Mechanism

Mounir Belkouch,[1,2] Marc-André Dansereau,[1] Annabelle Réaux-Le Goazigo,[2] Juliette Van Steenwinckel,[2] Nicolas Beaudet,[1] Ahmed Chraibi,[1]* Stéphane Melik-Parsadaniantz,[2]* and Philippe Sarret[1]*

[1]Department of Physiology and Biophysics, Faculty of Medicine and Health Sciences, Université de Sherbrooke, Sherbrooke, Quebec J1H 5N4, Canada, and [2]Pain Group, Centre de Recherche de l'Institut du Cerveau et de la Moelle Epinière, Université Pierre et Marie Curie, Inserm Unité Mixte de Recherche en Santé 975, Centre National de la Recherche Scientifique, Unité Mixte de Recherche 7225, 75013 Paris, France

Changes in function of voltage-gated sodium channels in nociceptive primary sensory neurons participate in the development of peripheral hyperexcitability that occurs in neuropathic and inflammatory chronic pain conditions. Among them, the tetrodotoxin-resistant (TTX-R) sodium channel $Na_v1.8$, primarily expressed by small- and medium-sized dorsal root ganglion (DRG) neurons, substantially contributes to the upstroke of action potential in these neurons. Compelling evidence also revealed that the chemokine CCL2 plays a critical role in chronic pain facilitation via its binding to CCR2 receptors. In this study, we therefore investigated the effects of CCL2 on the density and kinetic properties of TTX-R $Na_v1.8$ currents in acutely small/medium dissociated lumbar DRG neurons from naive adult rats. Whole-cell patch-clamp recordings demonstrated that CCL2 concentration-dependently increased TTX-resistant $Na_v1.8$ current densities in both small- and medium-diameter sensory neurons. Incubation with CCL2 also shifted the activation and steady-state inactivation curves of $Na_v1.8$ in a hyperpolarizing direction in small sensory neurons. No change in the activation and inactivation kinetics was, however, observed in medium-sized nociceptive neurons. Our electrophysiological recordings also demonstrated that the selective CCR2 antagonist INCB3344 [*N*-[2-[[(3*S*,4*S*)-1-*E*4-(1,3-benzodioxol-5-yl)-4-hydroxycyclohexyl]-4-ethoxy-3-pyrrolidinyl]amino]-2-oxoethyl]-3-(trifluoromethyl)benzamide] blocks the potentiation of $Na_v1.8$ currents by CCL2 in a concentration-dependent manner. Furthermore, the enhancement in $Na_v1.8$ currents was prevented by pretreatment with pertussis toxin (PTX) or gallein (a $G\beta\gamma$ inhibitor), indicating the involvement of $G\beta\gamma$ released from PTX-sensitive $G_{i/o}$-proteins in the cross talk between CCR2 and $Na_v1.8$. Together, our data clearly demonstrate that CCL2 may excite primary sensory neurons by acting on the biophysical properties of $Na_v1.8$ currents via a CCR2/$G\beta\gamma$-dependent mechanism.

Introduction

In sensory primary afferent neurons, voltage-gated sodium channels (VGSCs) are thought to play a critical role in the pathogenesis of chronic pain conditions (Amir et al., 2006; Dib-Hajj et al., 2010). Changes in the expression, trafficking, and function of VGSC have been particularly discussed to explain the neuronal hyperexcitability observed in the painful phenotype associated with nerve injury or peripheral inflammation (Docherty and Farmer, 2009; Swanwick et al., 2010). Several lines of evidence suggest that the tetrodotoxin-resistant (TTX-R) sodium channel $Na_v1.8$ mostly contributes to the enhanced excitability and spontaneous ectopic discharges occurring in small- and medium-sized dorsal root ganglion (DRG) neurons (Devor, 2006; Cummins et al., 2007; Dib-Hajj et al., 2009a). The enhanced responsiveness of these $Na_v1.8$-positive neurons thus leads to the development of hyperalgesia, allodynia, and ongoing spontaneous pain (Dib-Hajj et al., 2010; Lampert et al., 2010).

To date, several inflammatory mediators acting through G-protein-coupled receptors (GPCRs), including PGE_2, adenosine, and serotonin, have been shown to sensitize $Na_v1.8$ sodium channels and therefore to significantly increase the excitability of the nociceptor (Priest, 2009; Lampert et al., 2010). In addition to their well established role in the immune system, chemokines were also recently described to orchestrate the cellular response during the initiation/maintenance of chronic pain (Rittner and Brack, 2006; White et al., 2009; Gao and Ji, 2010). Among them, the chemokine CCL2 was shown to play a key role in spinal nociceptive processing, notably by sensitizing primary afferent neurons (Gosselin et al., 2008; White et al., 2009; White and Miller, 2010; Rostène et al., 2011). Acting via the binding to its cognate GPCR CCR2, intrathecal delivery of exogenous CCL2 was found

Received July 4, 2011; revised Oct. 28, 2011; accepted Oct. 28, 2011.

Author contributions: N.B., A.C., S.M.-P., and P.S. designed research; M.B., M.-A.D., A.R.-L.G., and J.V.S. performed research; M.B., N.B., A.C., S.M.-P., and P.S. analyzed data; M.B., N.B., A.C., S.M.-P., and P.S. wrote the paper.

This work was supported by a grant from the Canadian Institutes of Health Research (CIHR) (awarded to P.S. and S.M-P.). M.B. and M.-A.D. are supported by the Lavoisier and Sir Frederick Banting and Dr. Charles Best Canada Graduate Scholarships, respectively. P.S. is a CIHR new investigator. P.S. is director of the Sherbrooke's Neuroscience Center and a member of the Fonds de la Recherche en Santé du Québec-funded Centre de Recherche Clinique Étienne-Lebel.

*A.C., S.M.-P., and P.S. contributed equally to this work.

Correspondence should be addressed to Dr. Philippe Sarret, Department of Physiology and Biophysics, Faculty of Medicine and Health Sciences, Université de Sherbrooke, 3001, 12e Avenue Nord, Sherbrooke, Quebec J1H 5N4, Canada. E-mail: philippe.sarret@usherbrooke.ca.

DOI:10.1523/JNEUROSCI.3386-11.2011

Copyright © 2011 the authors 0270-6474/11/3118381-10$15.00/0

to promote pain hypersensitivity (Tanaka et al., 2004; Dansereau et al., 2008). Accordingly, CCL2-overexpressing or CCR2-deficient mice exhibited altered nociceptive behaviors to thermal, chemical, and mechanical stimuli (Abbadie et al., 2003; Menetski et al., 2007; Zhang et al., 2007). In addition, the use of CCR2 receptor antagonists or blocking antibodies successfully inhibited nociceptive signaling (Bhangoo et al., 2007, 2009; Dansereau et al., 2008; Serrano et al., 2010; Struthers and Pasternak, 2010; Van Steenwinckel et al., 2011). Similar to pain neuromodulators (Rostène et al., 2007), CCL2 is stored in large dense core vesicles known to contain pronociceptive-related peptides [substance P and CGRP (calcitonin gene-related peptide)], is released in a calcium-dependent manner from DRG neuronal cell bodies and terminal nerve endings, and directly excites primary nociceptive neurons by autocrine/paracrine processes (Oh et al., 2001; White et al., 2005; Sun et al., 2006; Dansereau et al., 2008; Jung et al., 2008; Van Steenwinckel et al., 2011).

Thus, the aim of the present study was to investigate whether the mechanism of CCL2-induced sensory neuron excitation might in part arise from the enhanced activation of TTX-R sodium channel $Na_v1.8$ currents. For this purpose, we examined the changes induced by CCL2 on the density and biophysical properties of $Na_v1.8$ currents in acutely dissociated small- and medium-sized DRG neurons from naive adult rats using whole-cell patch-clamp recordings. Additional electrophysiological studies were conducted to determine whether CCR2 receptor antagonist [*N*-[2-[[(3*S*,4*S*)-1-*E*4-(1,3-benzodioxol-5-yl)-4-hydroxycyclohexyl]-4-ethoxy-3-pyrrolidinyl] amino]-2-oxoethyl]-3-(trifluoromethyl)benzamide (INCB3344)] could inhibit the cross talk between CCR2 and $Na_v1.8$ (Brodmerkel et al., 2005). Finally, in light of the association of CCR2 with $G_{i/o}$-protein subunits (Bajetto et al., 2002), we further evaluated the molecular basis of this functional interaction by exploring the effects of signaling inhibitors on $Na_v1.8$ currents evoked by CCR2 activation.

Materials and Methods

Animals. Adult male Sprague Dawley rats (250–300 g) were housed two per cage in a climate-controlled room on a 12 h light/dark cycle with water and food *ad libitum*. All experimental procedures were approved by the Animal Care and Use Committee of the Université de Sherbrooke and were in accordance with the guidelines provided by the Canadian Council of Animal Care.

Acute culture of DRG neurons. DRG neurons from adult rats were acutely isolated as described previously (Zhou et al., 2003). Briefly, rats were exposed to CO_2 and decapitated. The bilateral L4–L5 DRGs were isolated, quickly unsheathed in calcium/magnesium-free PBS with glucose (1.6 M), and all adherent connective tissue was removed. Isolated DRGs were then enzymatically digested with collagenase A for 90 min (1 mg/ml; Roche Diagnostics) in PBS containing glucose, and then for 30 min with trypsin (0.25%) (Invitrogen). Subsequently, DRG neurons were mechanically dissociated by repeated trituration using a fine polished Pasteur pipette in culture medium containing 1:1 DMEM and Ham's F12 medium, supplemented with 10% fetal bovine serum (Invitrogen) and 1% penicillin (100 U/ml)/streptomycin (0.1 mg/ml). Isolated neurons were gently centrifuged (50 × *g* for 3 min), plated on poly-D-lysine/laminin-coated glass coverslips, and incubated at 37°C in a humidified 95% air/5% CO_2 atmosphere. All of the electrophysiological recordings or immunocytochemical experiments were performed within 14–20 h, a sufficient time to allow the cells to adhere to the plate. For the immunocytochemical detection, DRG neurons were fixed for 15 min with 4% paraformaldehyde (PFA) for further immunostaining. During the brief period of culture, DRG neurons displayed only short axonal processes (<10 μm), thus facilitating the voltage-clamp studies, and minimizing changes in electrical properties that can occur in long-term culture.

Immunofluorescence labeling. For tissue sections, rats were deeply anesthetized with sodium pentobarbital (50 mg/kg, i.p.) and perfused transaortically with saline, followed by 4% PFA containing 0.8% picric acid in 0.1 M PBS. Lumbar DRGs were rapidly dissected and postfixed in the same fixative overnight at 4°C. DRGs were then cryoprotected in 30% sucrose and frozen 1 min at −40°C in isopentane. DRGs were sliced using a cryostat in 12 μm (Jung CM 3100; Leica Microsystems) sections, and then mounted on Superfrost slides. To simultaneously detect CCR2 and $Na_v1.8$, tissue sections and cultured DRG neurons were processed for dual immunofluorescence labeling. Specimens were incubated in 0.1 M PBS containing 3% NGS and 0.1% Triton X-100 for 2 h, and then treated with a rabbit CCR2 antibody for 1 h (Gosselin et al., 2005). After rinsing three times with 0.1 M PBS, sections were incubated with a biotin-conjugated goat anti-rabbit antibody (1:1000; Vector Laboratories) for 1 h and finally revealed by incubation with streptavidin-Alexa Fluor 488 (1:1000; Invitrogen). Subsequently, cultured rat DRG neurons and L4–L6 DRG sections were incubated with a goat anti-rabbit IgG (Vector; 1:100) for 1 h to completely block sites of primary CCR2 antibody. Specimens were then treated with rabbit anti-$Na_v1.8$ (1:500; Alomone Labs) and stained with Alexa Fluor 555-conjugated goat anti-rabbit (1:1000; Invitrogen). Specimens were then washed and mounted with Aqua-mount. We performed primary and secondary antibody control experiments for each combination of primary and secondary antibodies, to evaluate nonspecific secondary antibody binding and cross-reactivity between primary and secondary antibodies. Experiments performed in the absence of primary and/or secondary antibody revealed an absence of immunofluorescence labeling (data not shown). Double-labeled sections were analyzed by light microscopy using a Zeiss fluorescence microscope (Carl Zeiss) fitted with highly discriminating filters. Pictures were taken using a digital camera (AxioCam HRC; Carl Zeiss) connected to an image acquisition software (AxioVision; Carl Zeiss).

cAMP assay. Acutely dissociated DRG neurons were dispensed into poly-D-lysine-coated 24-well plates (2×10^5 cells per well). After 16 h, cells were preincubated for 2 h at 37°C in 200 μl of Krebs'–Ringer's solution (10 mM HEPES, 118 mM NaCl, 2.5 mM $CaCl_2$, 4.75 mM KCl, 1.2 mM $MgSO_4$ 1.2 mM KH_2PO_4, 24 mM $NaHCO_3$, 11.1 mM glucose, and 0.3% BSA) in the presence or not of the G_i inhibitor, pertussis toxin (PTX) (250 ng/ml; Sigma-Aldrich). The medium was then replaced by 200 μl of Krebs'–Ringer's solution containing 0.1 mM 3-isobutyl-1-methylxanthine (IBMX) (Sigma-Aldrich), a nonspecific cyclic nucleotide phosphodiesterase inhibitor, and the cells were incubated for 15 min at 37°C. Then, 200 μl of a solution containing CCL2 (at a final concentration of 100 nM) were added to the medium, and the cells were incubated for another 30 min at 37°C. Basal levels were determined in parallel by incubating cells in the absence of CCL2 for 30 min at 37°C in 400 μl of Krebs'–Ringer's solution containing 0.1 mM IBMX. The reaction was stopped by replacing the incubation medium with 100 μl of 0.1N HCl for 20 min at room temperature. Next, the cells were scraped and centrifuged for 10 min at 10,000 rpm. Collected supernatants were then processed directly for cAMP determination by using the cAMP Direct Immunoassay kit (Abcam; ab65355), as recommended by the manufacturer.

Whole-cell patch-clamp recordings. Sodium currents were recorded from single, small- to medium-sized DRG neurons in the whole-cell patch-clamp configuration 14–20 h after dissociation and plating, using an Axopatch 200B amplifier (Molecular Devices). All experiments were performed at room temperature (21–23°C). The intracellular recording electrodes were made from borosilicate glass capillary tubes (Warner Instruments), pulled using a two-step vertical micropipette puller P83 (Narashige), and heat-polished on a microforge (Narashige).

The pipette solution contained the following (in mM): 10 NaCl, 140 CsCl, 10 EGTA, 1 $MgCl_2$, 2 Na_2ATP, 10 HEPES; pH was adjusted to 7.2 by CsOH. Osmolarity was adjusted to 310 mOsm/L with sucrose. Pipettes had a resistance of 2–4 MΩ when filled with the pipette solution. After formation of a tight seal (>1 GΩ), whole-cell access was obtained by rupturing the membrane, and membrane resistance and capacitance (C_m) were determined. Capacity transients were cancelled using computer-controlled circuitry and series resistance was compensated (>85%) in all experiments. The external solution contained the following (in mM): 35 NaCl, 65 NMDG-Cl, 30 tetraethylammonium (TEA)-Cl, 0.1 $CaCl_2$, 0.1 $CoCl_2$, 5 $MgCl_2$, 10 HEPES, and 10 glucose, pH adjusted at 7.4 by NaOH and osmolarity adjusted to 300 mOsm/L. The TEA-Cl and

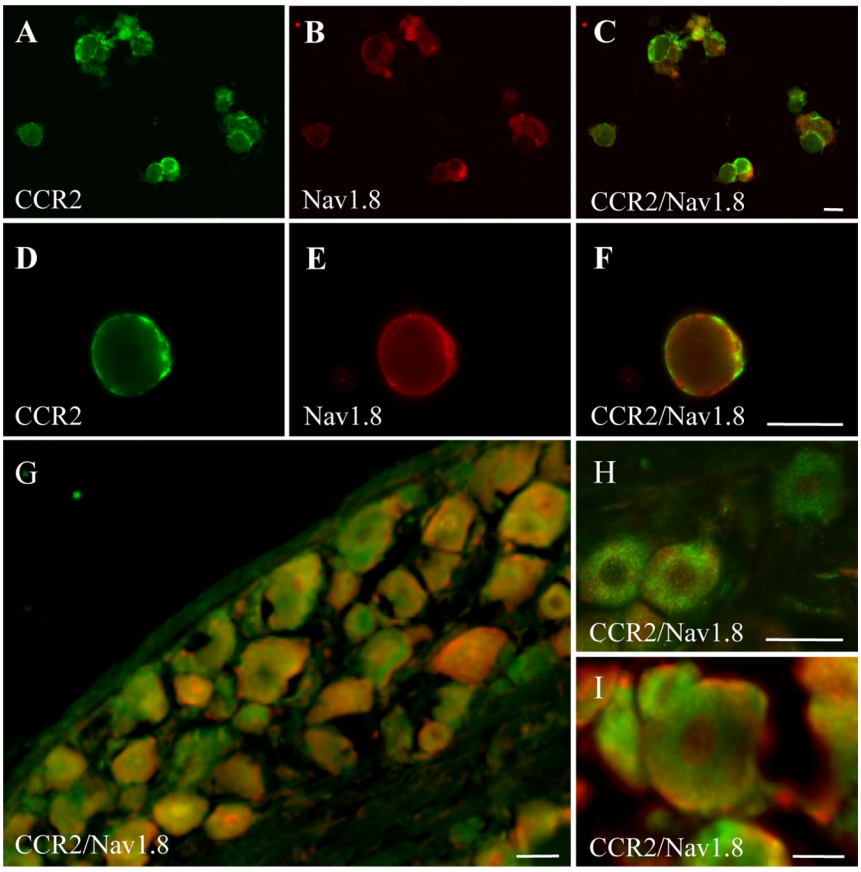

Figure 1. Cellular distribution of $Na_v1.8$ and CCR2 in rat DRG neurons. Immunofluorescence staining of CCR2 (green) (***A***, ***D***) and $Na_v1.8$ (red) (***B***, ***E***) on acutely dissociated primary afferent neurons. The merged images show dually labeled small- and medium-sized sensory neurons (yellow) (***C***, ***F***). Note that CCR2 and $Na_v1.8$ are mainly detected at the periphery of the cell. Immunohistochemical labeling performed on DRG sections from naive rats (***G–I***). Numerous small- to medium-diameter DRG neurons display both $Na_v1.8$ and CCR2 immunoreactivities. Scale bars, 20 μm.

$CoCl_2$ were used to inhibit endogenous K^+ and Ca^{2+} currents, respectively. The external sodium concentration was reduced to 35 mM to maintain adequate clamp of currents and to ensure that the particular current under study was stable. Note that the amplitude of Na^+ currents was not affected over the time period used to record the effects of the different drugs.

Using a whole-cell configuration, TTX-R $Na_v1.8$ currents were isolated by prepulse inactivation as described previously (MeLean et al., 1988; Roy and Narahashi, 1992; Cummins and Waxman, 1997). Briefly, standard current–voltage (*I–V*) families were constructed using a holding potential of −120 mV with 500 ms prepulses to −50 mV before each depolarization to inactivate the fast TTX-sensitive (TTX-S) currents. Thus, standard *I–V* curves were obtained by the application of a series of test pulses to voltages that ranged from −70 to +40 mV in 10 mV increments after the prepulse inactivation protocol (see Fig. 2). The voltage dependence of inactivation was measured by applying a double-pulse protocol consisting of a 500 ms conditioning potential (−120 to −10 mV, 5 mV increments) followed by a fixed test pulse (−10 mV, 50 ms). The current amplitude (*I*) was normalized to the maximum control current amplitude (I_{max}).

Drugs. CCL2 (PeproTech) was applied at two different concentrations (10 and 100 nM) to the chamber for 30 min before patch-clamp recordings. Cultured DRG neurons were also treated with 100 nM CCL2 in the presence of increasing concentrations (1–100 nM) of the CCR2 antagonist INCB3344 (Global Pfizer; Pure Substance Program). DRG cells were also pretreated overnight with PTX (250 ng/ml) or with gallein, a specific G$\beta\gamma$ dimer signaling inhibitor (20 μM; Tocris Bioscience).

Data analysis and statistics. The peak inward current values at each potential were plotted to generate *I–V* curves. Conductance (*G*) was determined as $I/(V_m - V_{rev})$, where *I* is the current, V_m is the potential at which current is evoked, and V_{rev} is the reversal potential of the current. Activation was fitted with the following Boltzmann equation: $G = G_{max}/[1 + \exp[(V_{1/2} - V_m)/k]]$, where V_m is the test pulse voltage potential at which current is evoked, G_{max} is the calculated maximal conductance, $V_{1/2}$ is the potential of half-activation or inactivation, and *k* is the slope factor. The normalized curves were fitted using a Boltzmann distribution equation as follows: $I = I_{max}/[1 + \exp[(V_{1/2} - V_m)/k]]$, where I_{max} is the peak sodium current elicited after the most hyperpolarized prepulse, V_m is the preconditioning pulse potential, $V_{1/2}$ is the half-maximal sodium current, and *k* is the slope factor. INCB3344 dose–response curve was obtained by bracketing the responses to different INCB3344 concentrations (1–100 nM).

Recording data were acquired using a Digidata 1440 A series interface (Molecular Devices) digitized at 10 kHz, low-pass filtered at 2 kHz, and captured using pClamp software (version 10.2; Molecular Devices). For current density measurements, the currents were divided by the cell capacitance (C_m) as read from the amplifier. Cells were selected for recording based on whole-cell capacitance ($C_m < 30$ pF corresponding to small neurons, <25 μm; $C_m <$ 55 pF corresponding to medium neurons, <25–32 μm). The offset potential was zeroed before patching the cells and leakage current was digitally subtracted on-line using hyperpolarizing potentials, applied after the test pulse.

Data are expressed as means ± SEM. Statistical analyses were performed using Student's *t* test or one-way ANOVA followed by Dunnett's posttest. A value of $p < 0.05$ was considered statistically significant. Curves were fitted using Origin software (OriginLab Corporation), and graphs were plotted using GraphPad, version 5.d (GraphPad Software). Final composites were processed using Deneba's Canvas 10.5 imaging software (Deneba Software).

Results

Colocalization of $Na_v1.8$ and CCR2 in cultured rat sensory neurons and DRG tissue

To determine whether $Na_v1.8$ was present within the same sensory neuronal population as CCR2, dual immunofluorescence labeling was performed on dissociated primary afferent neurons and on DRG sections from naive rats (Fig. 1). Dual immunostaining revealed that $Na_v1.8$ and CCR2 colocalized extensively over small- to medium-sized sensory neurons (Fig. 1*A–F*). At higher magnification, the distribution patterns for both $Na_v1.8$ and CCR2 were entirely restricted to the periphery of the neuron somata (Fig. 1*D–F*). Accordingly, fluorescence microscopy performed on DRG tissue sections revealed that numerous $Na_v1.8$-positive small and medium sensory neurons were also immunoreactive for CCR2 (Fig. 1*G–I*). In addition, CCR2 and $Na_v1.8$ immunoreactivities were detected in axonal fibers in DRG sections, suggesting anterograde transport of both proteins to nerve terminals (data not shown). The presence of CCR2 receptors on $Na_v1.8$-positive neurons led us to investigate, by electrophysiological approaches, whether the CCR2 ligand CCL2 could modulate the TTX-resistant $Na_v1.8$ currents.

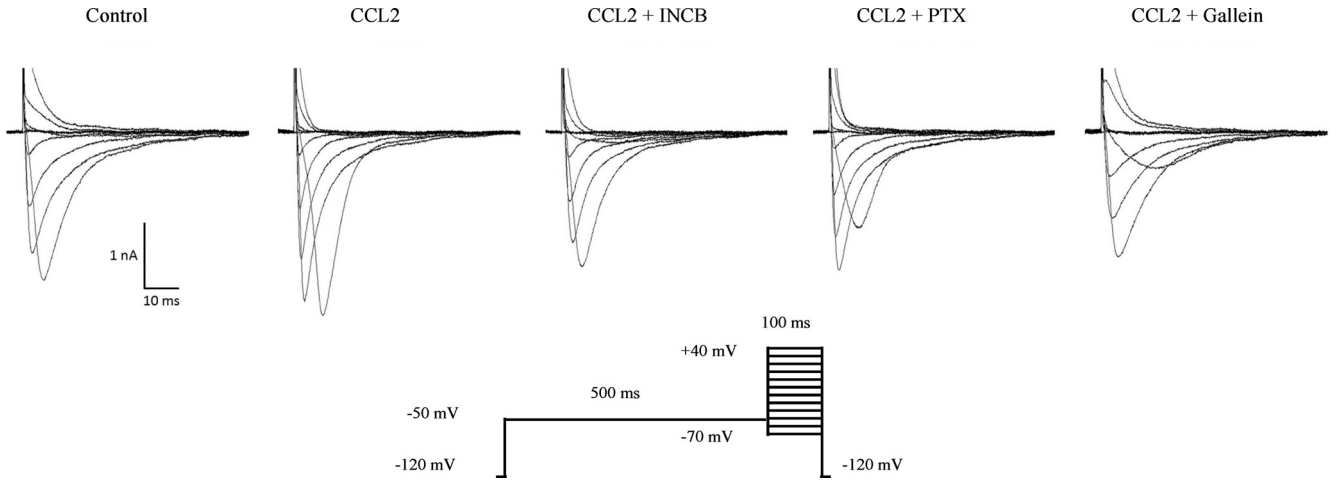

Figure 2. Isolation of TTX-resistant $Na_v1.8$ currents in small-sized rat sensory neurons. Whole-cell voltage-clamp current traces of $Na_v1.8$ in small-diameter sensory neurons recorded following a 30 min incubation with 100 nM CCL2 in the absence ($n = 11$) or presence of INCB3344 (100 nM; $n = 7$), PTX (250 ng/ml; $n = 9$), or gallein (20 μM; $n = 6$). Representative *I–V* curves of currents are determined using the pulse protocol indicated in the inset.

CCL2 enhances $Na_v1.8$ currents in small primary sensory neurons

Several protocols exist to isolate TTX-R from TTX-S sodium currents. Here, we applied a prepulse inactivation protocol with a 500 ms step of −50 mV to isolate the slow-inactivating TTX-R sodium currents (MeLean et al., 1988; Roy and Narahashi, 1992; Cummins and Waxman, 1997). Furthermore, the membrane potential was held at −70 mV to inhibit $Na_v1.9$ currents, leaving the $Na_v1.8$ current intact (Rush et al., 2005; Cang et al., 2009). The family of $Na_v1.8$ sodium currents was generated with a voltage-clamp protocol by applying a range of potentials between −70 and +40 mV for 100 ms (Fig. 2). Using a whole-cell patch-clamp configuration, we therefore examined the effects of CCL2 on the density and kinetic properties of TTX-R $Na_v1.8$ currents in acutely dissociated lumbar DRG neurons. $Na_v1.8$ current amplitude was increased in small neurons (C-fibers) following an incubation of 30 min with 100 nM CCL2 (Fig. 2). Under these conditions, current–voltage (*I–V*) analysis revealed that the mean peak current amplitude was significantly higher in CCL2-treated (−99.13 ± 2.77 pA/pF; $n = 11$) than in control DRG neurons (−53.30 ± 2.15 pA/pF; $n = 13$) (Fig. 3*A*,*B*; $^{***}p < 0.001$). The peak current density was also affected significantly at the lowest concentration of CCL2 (10 nM) (−63.55 ± 12.26 pA/pF; $n = 4$; $^{*}p < 0.05$; Fig. 3*A*,*B*).

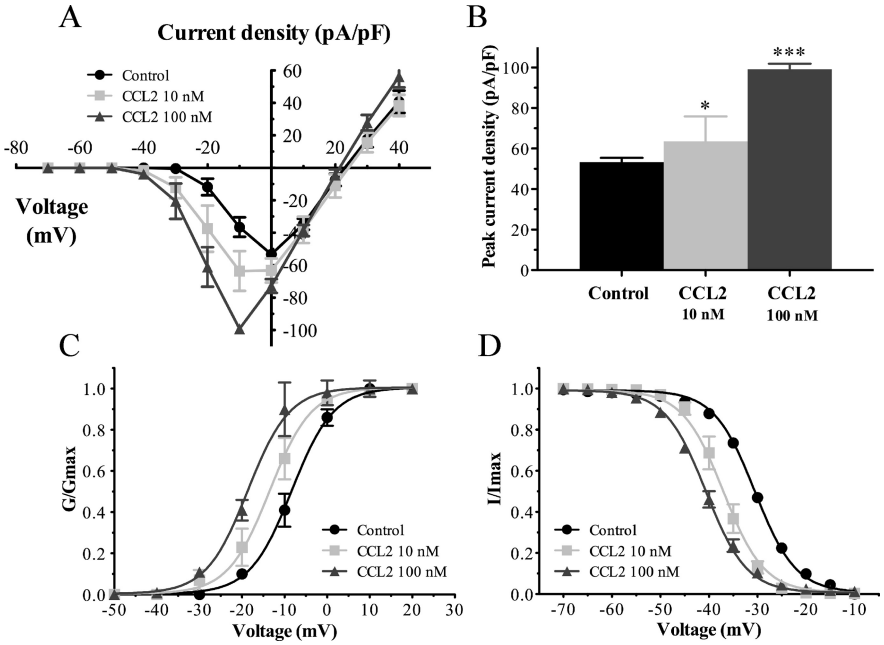

Figure 3. $Na_v1.8$ currents are increased in small sensory neurons following exposure to CCL2. ***A***, Current–voltage relationships of $Na_v1.8$ were determined before (black circles) and after application of 10 nM (gray squares) or 100 nM (gray triangles) of CCL2. ***B***, Peak $Na_v1.8$ current densities were significantly enhanced in the presence of 10 and 100 nM CCL2 ($^{*}p < 0.05$ and $^{***}p < 0.001$, respectively, vs control; Student's *t* test; $n = 6–13$). Error bars indicate SEM. ***C***, ***D***, CCL2 shifted the activation (***C***) and steady-state inactivation (***D***) curves in a hyperpolarizing direction. The midpoint values of the activation ($V_{1/2act}$) and inactivation ($V_{1/2inact}$) curves are illustrated in Table 1.

Acute application of 100 nM CCL2 also shifted the activation and steady-state inactivation curves of $Na_v1.8$ in a hyperpolarizing direction (Fig. 3*C*,*D*). The midpoint of activation ($V_{1/2act}$) was significantly decreased in CCL2-treated neurons compared with control neurons (−18.74 ± 0.31 mV, $n = 11$, vs −8.45 ± 0.21 mV, $n = 13$, respectively; $^{***}p < 0.001$) (Fig. 3*C*, Table 1). The slope factor (k_{act}) was not affected by CCL2 perfusion ($k_{control} = 4.73 \pm 0.19$ vs $k_{CCL2} = 4.47 \pm 0.29$ mV; Table 1). Similar to the activation curve, the steady-state inactivation parameter, *hinf*, was significantly influenced by the presence of CCL2 (Fig. 3*D*). Indeed, the half-inactivation potential ($V_{1/2inact}$) was shifted to −40.61 ± 0.09 mV ($n = 10$) from that of control condition (−30.55 ± 0.17 mV; $n = 10$) after 100 nM CCL2 treatment ($^{***}p < 0.001$; Table 1). Slope values (k_{inact}) remained unchanged between CCL2-treated (4.81 ± 0.08 mV) and control (4.72 ± 0.15 mV) neurons. Moreover, lower concentration of CCL2 (10 nM) caused a left shift in the activation ($V_{1/2act} = -13.72 \pm 0.22$ mV; $n = 4$; $^{*}p < 0.05$) and steady-state inactivation ($V_{1/2inact} = -37.02 \pm 0.16$ mV; $n = 7$; $^{**}p < 0.01$) curves of $Na_v1.8$ (Fig. 3*C*,*D*; Table 1).

Table 1. Activation and steady-state inactivation characteristics of $Na_v1.8$ currents in small-diameter sensory neurons

	$V_{1/2act}$ (mV)	k_{act}	$V_{1/2inact}$ (mV)	k_{inact}
Control	−8.45 ± 0.21 ($n = 13$)	4.73 ± 0.19	−30.55 ± 0.17 ($n = 10$)	4.72 ± 0.15
CCL2 (10 nM)	−13.72 ± 0.22* ($n = 4$)	3.5 ± 0.19	−37.02 ± 0.16** ($n = 7$)	3.66 ± 0.14
CCL2 (100 nM)	−18.74 ± 0.31*** ($n = 11$)	4.47 ± 0.29	−40.61 ± 0.09*** ($n = 10$)	4.81 ± 0.08
CCL2 (100 nM) + INCB3344 (100 nM)	−7.47 ± 0.26## ($n = 7$)	5.01 ± 0.23	−31.02 ± 0.16### ($n = 5$)	3.59 ± 0.14
CCL2 (100 nM) + PTX (250 ng/ml)	−7.04 ± 0.22## ($n = 9$)	4.14 ± 0.20	ND	ND
CCL2 (100 nM) + gallein (20 μM)	−6.09 ± 0.22### ($n = 6$)	4.10 ± 0.17	ND	ND

$V_{1/2act}$ and $V_{1/2inact}$ are the membrane potentials for half-maximal channel activation or inactivation, respectively. k_{act} and k_{inact} represent the slope factors for activation and inactivation. The numbers in parentheses reflect numbers of recorded neurons. ND, Not determined.

$^{**}p < 0.01$ and $^{***}p < 0.001$ indicate statistically significant differences with control group. $^{\#\#}p < 0.01$ and $^{\#\#\#}p < 0.001$ compared with CCL2 alone.

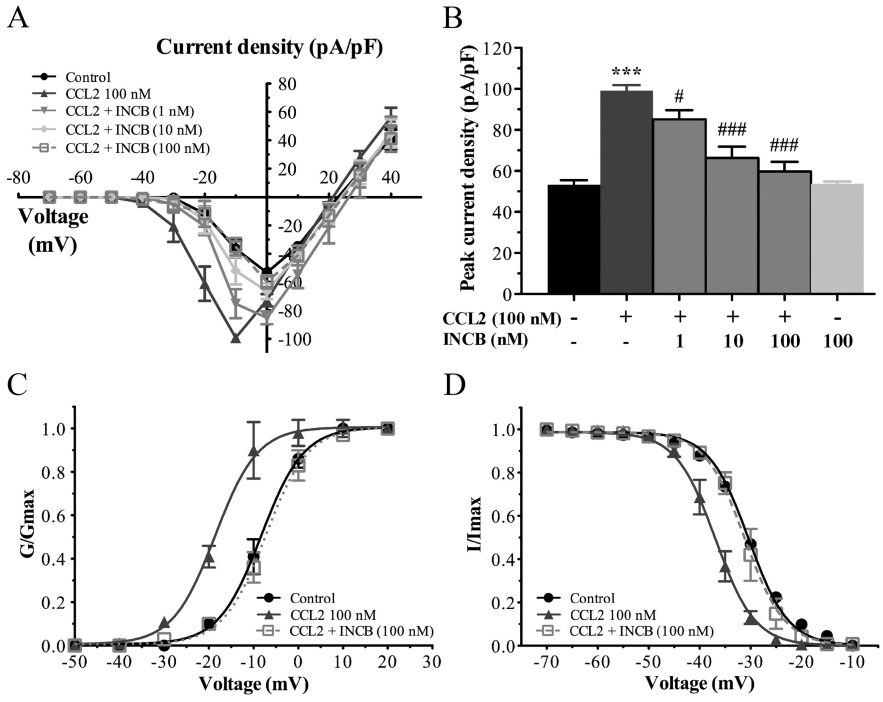

Figure 4. INCB3344 treatment blocks the changes in the biophysical properties of $Na_v1.8$ induced by CCL2. ***A***, *I–V* curves of $Na_v1.8$ currents obtained from small rat DRG neurons. ***B***, Histogram showing the effects of different concentrations of INCB3344 (1, 10, 100 nM) on the increased $Na_v1.8$ peak current induced by 100 nM CCL2 ($^{***}p < 0.001$, CCL2 alone vs control; $^{\#\#\#}p < 0.001$, $^{\#}p < 0.05$, INCB3344 plus CCL2 vs CCL2 alone; Student's *t* test; $n = 6–11$; pound signs correspond to the values in the Table 1). Error bars indicate SEM. ***C***, ***D***, INCB3344 also significantly inhibits the leftward shift of the activation (***C***) ($^{\#\#}p < 0.01$) and inactivation (***D***) ($^{\#\#\#}p < 0.001$ compared with CCL2 alone) curves of $Na_v1.8$ current observed in the presence of 100 nM CCL2. The experimental conditions corresponding to control and 100 nM CCL2 have already been presented in Figure 3. Half-activation and half-inactivation potentials and slope factors are summarized in Table 1.

Potentiation of $Na_v1.8$ currents by CCL2 is blocked by the selective CCR2 antagonist

We then investigated whether these changes in the biophysical properties of $Na_v1.8$ currents induced by CCL2 application were directly mediated by CCR2. For this purpose, electrophysiological recordings were performed on small sensory neurons following 30 min preincubation with 100 nM CCL2, in the presence of increasing concentrations of the CCR2 antagonist INCB3344 (ranging from 1 to 100 nM). As shown in Figure 2, the increase in CCL2-induced $Na_v1.8$ sodium currents was considerably reduced in the presence of 100 nM INCB3344, thus demonstrating that the effects of CCL2 were CCR2 dependent. *I–V* curves of $Na_v1.8$ currents also revealed that coincubation with INCB3344 produced a concentration-dependent inhibition of the mean peak current density, with an IC_{50} of 21 nM (Fig. 4*A*,*B*). At the highest concentration tested (100 nM), the selective CCR2 antagonist decreased by 85% the peak amplitude of $Na_v1.8$ current evoked by CCL2 (−99.13 ± 2.77 pA/pF, $n = 11$, for CCL2, vs −59.77 ± 4.65 pA/pF, $n = 7$, for CCL2 plus INCB3344; $^{\#\#\#}p < 0.001$; Fig. 4*A*,*B*). No significant change in $Na_v1.8$ current density or kinetics was seen when INCB3344 (100 nM) was applied alone (Fig. 4*B*).

The changes in the activation and steady-state inactivation curves of $Na_v1.8$ observed under CCL2 stimulation (100 nM) were also prevented by the presence of INCB3344. Indeed, INCB3344 at 100 nM fully blocked the left shift in the activation curves of $Na_v1.8$ induced by CCL2 (−18.74 ± 0.31 mV, $n = 11$, for CCL2, vs −7.47 ± 0.26 mV, $n = 7$, for CCL2 plus INCB3344) ($^{\#\#}p < 0.01$; Fig. 4*C*, Table 1). In addition, the hyperpolarizing shift in the inactivation curve of TTX-R $Na_v1.8$ currents observed in response to CCL2 returned to baseline values following coincubation with the CCR2 antagonist. The half-inactivation potential was −40.61 ± 0.09 mV using CCL2 alone ($n = 10$), and −31.02 ± 0.16 mV when incubating with 100 nM INCB3344 ($^{\#\#\#}p < 0.001$; $n = 5$) (Fig. 4*D*, Table 1). The slope factors, k_{act} and k_{inact} were unaltered by the presence of INCB3344 (Table 1).

$G_{i/o}$-proteins participate in CCL2-induced $Na_v1.8$ current activation

CCR2 activation by CCL2 initiates intracellular signaling cascades among the ones coupling to heterotrimeric G-proteins of the G_i family (Bajetto et al., 2002; Gosselin et al., 2008). Before determining the possible role of $G_{i/o}$-proteins in the CCL2 activation of $Na_v1.8$ current, we have first examined whether CCL2 activated CCR2 through a $G_{i/o}$-coupled mode of action to decrease neuronal cAMP production and whether treatment with the irreversible inhibitor of $G_{i/o}$-proteins, PTX (250 ng/ml) inhibited the functional coupling of CCR2 to adenylyl cyclase. As shown in Figure 5*A*, CCL2 applied at a concentration of 100 nM to dissociated primary sensory neurons significantly decreased basal levels of cAMP up to 30% ($^{*}p < 0.05$). Moreover, overnight pretreatment with PTX reversed by 70% the CCL2-induced inhibition of adenylyl cyclase activity ($^{\#}p < 0.05$), thus demonstrating that CCR2 activation modulates the neuronal cAMP levels in a $G_{i/o}$-protein-dependent manner.

We next determined whether PTX treatment of acutely dissociated sensory neurons affected CCL2-induced $Na_v1.8$ current activation. Our results revealed that overnight incubation with

PTX significantly prevented the $Na_v1.8$ current amplitude change induced by 100 nM CCL2, indicating that the influence of CCL2 on $Na_v1.8$ is dependent of the trimeric G_i-protein complex (Fig. 2). The peak current densities were -99.13 ± 2.77 pA/pF ($n = 11$) and -52.37 ± 3.09 pA/pF ($n = 9$) before and after application of PTX, respectively ($^{###}p < 0.001$; Fig. 5*B*,*C*). Applied alone, PTX caused no significant changes in the $Na_v1.8$ current amplitude (Fig. 5*C*). In addition, the hyperpolarized shift in the midpoint of activation, observed upon CCL2 stimulation ($V_{1/2act} = -18.74 \pm 0.31$ mV; $n = 11$) was completely inhibited in the presence of PTX ($V_{1/2act} = -7.04 \pm 0.22$ mV; $n = 9$) ($^{##}p < 0.01$; Fig. 5*D*, Table 1). The k_{act} value was not changed by PTX treatment (Table 1).

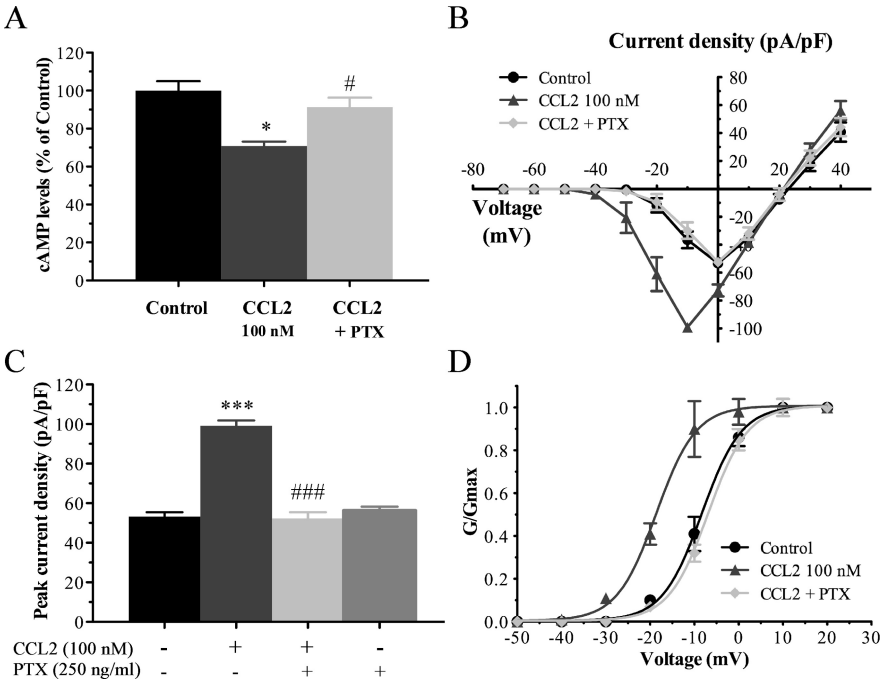

Figure 5. Involvement of $G_{i/o}$-proteins in CCL2-induced potentiation of $Na_v1.8$ currents. ***A***, Neuronal cAMP measurement following application of CCL2 in the presence or absence of PTX. CCL2-induced inhibition of adenylyl cyclase activity is blunted by PTX pretreatment ($^{*}p < 0.05$, CCL2 alone vs control; $^{\#}p < 0.05$, PTX plus CCL2 vs CCL2 alone; one-way ANOVA followed by Dunnett's posttest, performed in triplicate). Error bars indicate SEM. ***B***, ***C***, *I–V* curves (***B***) and histogram (***C***) showing the action of CCL2 on $Na_v1.8$ currents ($^{***}p < 0.001$ compared with Control; Student's *t* test) and the inhibition of this effect with PTX (250 ng/ml) pretreatment ($^{###}p < 0.001$ compared with CCL2 alone; Student's *t* test; $n = 7$–11). ***D***, Preincubation with PTX also impedes the action of CCL2 on the normalized conductance ($^{##}p < 0.01$; G/G_{max}). Note that the experimental conditions corresponding to control and 100 nM CCL2 have been shown previously in Figure 3.

CCL2 activates $Na_v1.8$ currents through the release of G$\beta\gamma$ dimers

There is ample evidence in the literature demonstrating that G-protein $\beta\gamma$ subunits released from some GPCR upon receptor activation regulate a variety of downstream pathways to control various physiological functions (Smrcka et al., 2008). As a classical GPCR, CCR2 has also been shown to modulate different signaling pathways through the release of G$\beta\gamma$ (Bajetto et al., 2002). Therefore, we next determined the potential role of G$\beta\gamma$ in CCL2-mediated $Na_v1.8$ activation. Dissociated primary sensory neurons were thus incubated overnight with 20 μM gallein, a specific G$\beta\gamma$ dimer signaling inhibitor (Lehmann et al., 2008; Irannejad and Wedegaertner, 2010; Ukhanov et al., 2011). As shown in Figure 2, the increase in CCL2-induced $Na_v1.8$ sodium currents was blocked by gallein pretreatment. Under CCL2 stimulation, the peak current densities were -99.13 ± 2.77 pA/pF ($n = 11$) and -50.63 ± 1.73 pA/pF ($n = 6$) before and after application of gallein, respectively ($^{###}p < 0.001$; Fig. 6*A*,*B*). Inhibition of G$\beta\gamma$ also completely prevented the leftward shift in the activation curves of $Na_v1.8$ induced by CCL2 (-18.74 ± 0.31 mV, $n = 11$, for CCL2, vs -6.09 ± 0.22 mV, $n = 6$, for CCL2 plus gallein) ($^{###}p < 0.001$; Fig. 6*C*, Table 1). The $Na_v1.8$ current amplitude was not changed following application of gallein alone (Fig. 6*B*).

Regulation of $Na_v1.8$ currents by CCL2 in medium-sized primary sensory neurons

As shown in Figure 1, *G–I*, $Na_v1.8$ channels are also expressed by medium-sized primary sensory neurons. We thus evaluated whether the biophysical properties of $Na_v1.8$ current were differently affected in medium-diameter primary sensory neurons compared with small sensory neurons. Whole-cell patch-clamp recordings demonstrated that CCL2 significantly increased TTX-resistant $Na_v1.8$ current densities in dissociated medium DRG neurons of naive rats (Fig. 7). The mean current amplitude at 0 mV was significantly higher after 100 nM CCL2 application (-82.60 ± 4.24 pA/pF; $n = 11$) compared with untreated DRG neurons (-62.19 ± 1.55 pA/pF; $n = 18$) (Fig. 8; $^{***}p < 0.001$). Peak current densities were also significantly reduced following exposure to INCB3344 (-64.38 ± 3.03 pA/pF; $n = 7$; $^{###}p < 0.001$), PTX (-62.23 ± 7.62 pA/pF; $n = 5$; $^{\#}p < 0.05$), or gallein (-62.60 ± 1.43 pA/pF; $n = 11$; $^{###}p < 0.001$) (Figs. 7, 8). Unlike small-sized neurons, there was, however, no change in the activation and steady-state inactivation curves of $Na_v1.8$ following CCL2 treatment (Fig. 8*C*, Table 2).

Discussion

Reports on the CCL2/CCR2 chemokine/receptor complex in a number of chronic pain disorders led us to investigate the peripheral mechanisms of CCL2-induced pain facilitation (Rostène et al., 2007; White et al., 2009). Using whole-cell patch-clamp recordings, we demonstrated here that CCL2 enhanced $Na_v1.8$ current densities in both small- and medium-sized acutely dissociated sensory neurons. We also found that CCL2 increased excitability in small sensory neurons by shifting the activation and steady-state inactivation curves of $Na_v1.8$ in the hyperpolarizing direction. This increase in $Na_v1.8$ current was blocked by the selective CCR2 antagonist. This confirms that CCR2 is directly involved in CCL2-induced changes in $Na_v1.8$ activity. We also found that the G$\beta\gamma$ released from PTX-sensitive $G_{i/o}$ proteins is primarily responsible for the activation of $Na_v1.8$ currents in response to CCL2 in primary sensory neurons.

Neuromodulation of $Na_v1.8$ sodium channels by CCL2

Sustained pain hypersensitivity and neuronal hyperexcitability associated with nerve injury or disease-induced inflammatory responses of the peripheral nervous system are believed to result from chronic changes within DRG. In particular, modulation of voltage-gated sodium channels may underlie the increased excit-

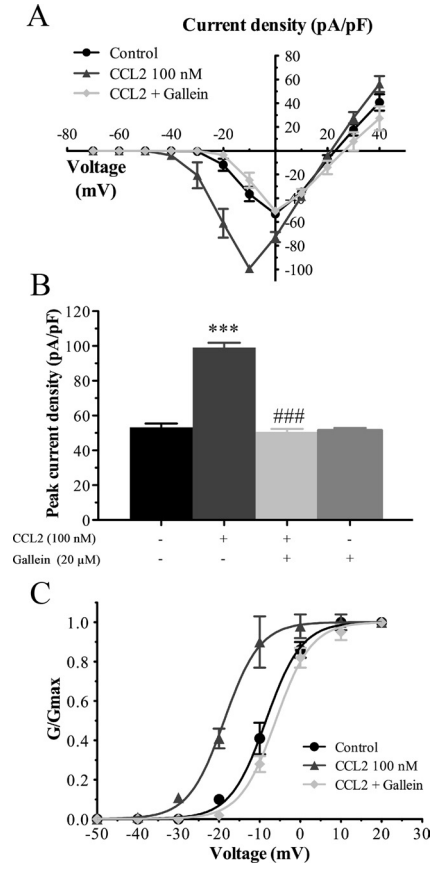

Figure 6. $G\beta\gamma$ participates in CCL2-induced $Na_v1.8$ currents. ***A***, ***B***, *I–V* curves (***A***) and histogram (***B***) of $Na_v1.8$ currents obtained from small rat DRG neurons showing that pretreatment with the $G\beta\gamma$ inhibitor gallein (20 μM) prevents the effects of CCL2 on $Na_v1.8$ currents ($^{***}p < 0.001$, CCL2 alone vs control; $^{###}p < 0.001$ gallein plus CCL2 compared with CCL2 alone; Student's *t* test; $n = 6–11$). Error bars indicate SEM. ***C***, Gallein also completely reverses the leftward shift of activation curve of $Na_v1.8$ observed in the presence of 100 nM CCL2 ($^{###}p < 0.001$). Note that the experimental conditions corresponding to control and 100 nM CCL2 have been shown previously in previous figures. Half-activation and half-inactivation potentials and slope factors are summarized in Table 1.

ability of primary afferent neurons (Dib-Hajj et al., 2009b; Docherty and Farmer, 2009; Swanwick et al., 2010). Among them, $Na_v1.8$ has emerged as a key contributor to action potential generation in nociceptors (Cummins et al., 2007; Dib-Hajj et al., 2009a). In support, functional knockdown of $Na_v1.8$ in rats or deletion of the $Na_v1.8$ gene reduces hyperalgesia and allodynia in neuropathic pain models (Dib-Hajj et al., 2010; Lampert et al., 2010). Likewise, systemic and spinal administrations of $Na_v1.8$ channel blockers partially reverse pain-related behaviors in preclinical animal models of chronic pain (Bear et al., 2009; Bhattacharya et al., 2009; Matulenko et al., 2009; Priest, 2009). Although $Na_v1.8$ antagonists may have analgesic efficacy in patients coping with chronic pain, the high degree of structural homology within the VGSC family and side effects of existing blockers have limited their clinical use (England, 2008; Dworkin et al., 2010). Given the fact that it is actually difficult to selectively target $Na_v1.8$, alternatives have been proposed like the indirect regulation of $Na_v1.8$ function by acting upstream via GPCR inhibition. In that respect, inflammatory mediators, such as prostaglandin, adenosine, and serotonin have been shown to influence both activity and trafficking of TTX-R sodium channels (Gold et al., 1996; Rush and Waxman, 2004; Liu et al., 2010; Ebersberger et al., 2011).

Considerable data support the hypothesis that proinflammatory chemokines induce pain hypersensitivity, notably by causing sensory neuron hyperactivity (Wang et al., 2008; Miller et al., 2009; White et al., 2009). Accordingly, the intraganglionic release of CCL2 strongly excites CCR2-expressing nociceptive DRG neurons (Oh et al., 2001; White et al., 2005; Sun et al., 2006; Jung et al., 2008). The depolarization of these sensory neurons thus implies that a number of ion channels may be downstream targets of CCR2 activation. Here, we therefore investigated whether the chemokine CCL2 contributed to nociceptive neurons excitability through the enhancement of $Na_v1.8$ currents. We first observed by dual immunofluorescence staining that, in both acutely dissociated cells and DRG sections, CCR2 receptors were present in most small- to medium-sized sensory neurons, previously described to express $Na_v1.8$ (Lai et al., 2004; Devor, 2006; Cummins et al., 2007; Dib-Hajj et al., 2009a). Consistently, we demonstrated using whole-cell patch-clamp recordings that acute application of CCL2 to small DRG neurons concentration-dependently increased the magnitude of $Na_v1.8$ currents and triggered a hyperpolarizing shift of both activation and inactivation curves. Interestingly, patch-clamp recordings from medium-sized DRG neurons revealed that CCL2 also enhanced the peak current amplitude of $Na_v1.8$ but was, however, inefficient in shifting the conductance–voltage and the steady-state inactivation curves to more hyperpolarized potentials. Thus, these results reveal that CCL2 affects the functional properties of $Na_v1.8$ in a cell type-specific manner within peripheral sensory ganglia.

Transactivation of $Na_v1.8$ is not the only CCL2-mediated mechanism that is likely to be important in the excitation of sensory neurons. Indeed, TRP cation channels, TRPV1 and TRPA1, participate in CCL2-induced nociceptor sensitization (Jung et al., 2008). Similarly, inhibition of voltage-dependent K^+ conductance has been hypothesized to arise from the action of CCL2 within DRG (Sun et al., 2006). In addition to sensory neuron modulation, CCL2 spinally released may also contribute to the maintenance of central sensitization by potentiating the activity of NMDA and AMPA receptors or by causing GABAergic disinhibition (Gosselin et al., 2005; Gao et al., 2009). The data reported here argue that $Na_v1.8$ channels are targets of CCL2-induced signaling pathway and that the mechanisms by which CCL2 enhances neuronal excitability depend on the subset of DRG neurons.

Functional significance of CCR2 receptor activation to the modulation of $Na_v1.8$ channel

To date, several lines of evidence support a critical role of CCL2/CCR2 in promoting behavioral changes associated with chronic pain (Miller et al., 2009; White and Miller, 2010). In particular, the recent progress in identifying CCR2 antagonists has revealed their effectiveness in reversing the nociceptive behaviors induced by focal nerve demyelination injury or HIV sensory neuropathy (Bhangoo et al., 2007, 2009; Jung et al., 2009). Accordingly, we recently demonstrated that the selective CCR2 antagonist INCB3344 prevented the pronociceptive action of exogenous intraspinal CCL2 and attenuated tactile allodynia in nerve-injured rats (Dansereau et al., 2008; Van Steenwinckel et al., 2011). Here, we therefore evaluated whether treatment of small- and medium-sized sensory neurons with INCB3344 abolished CCL2-induced $Na_v1.8$ current activation. Our results demonstrated that application of INCB3344 concentration-dependently blocks CCL2-induced changes in $Na_v1.8$ current density or kinetics. Supporting the behavioral observations, these data clearly indicate that CCL2-induced pain facilitation is mediated by direct activation of CCR2 and that

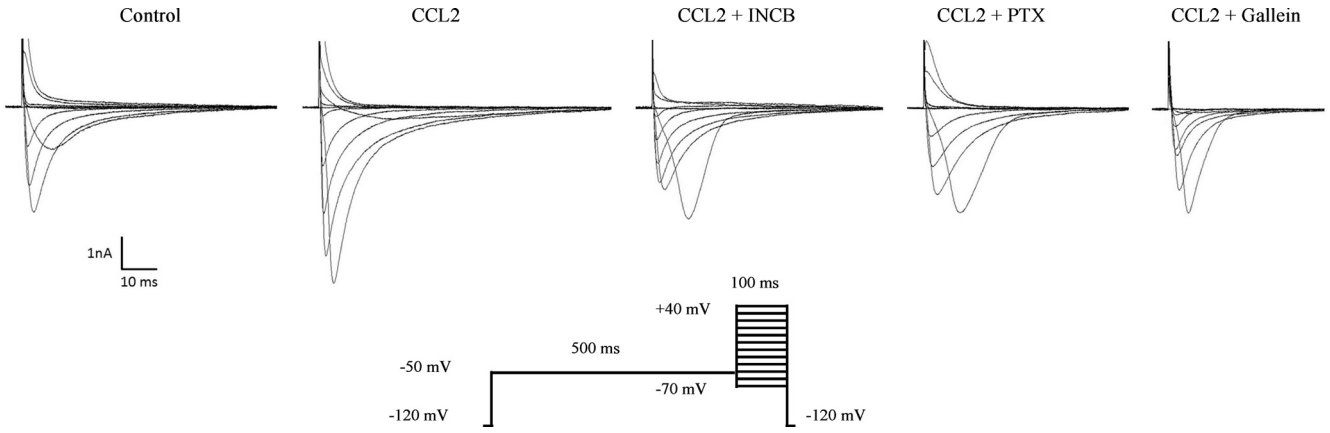

Figure 7. Representative families of $Na_v1.8$ sodium currents in medium-sized sensory neurons. Average *I–V* curve family of currents recorded from medium neurons under CCL2 stimulation alone (100 nM; $n = 11$), and in the presence of INCB3344 (100 nM; $n = 7$), PTX (250 ng/ml; $n = 5$), or gallein (20 μM; $n = 11$). INCB3344, PTX, and gallein all efficiently reverse CCL2-induced enhancement of $Na_v1.8$ currents.

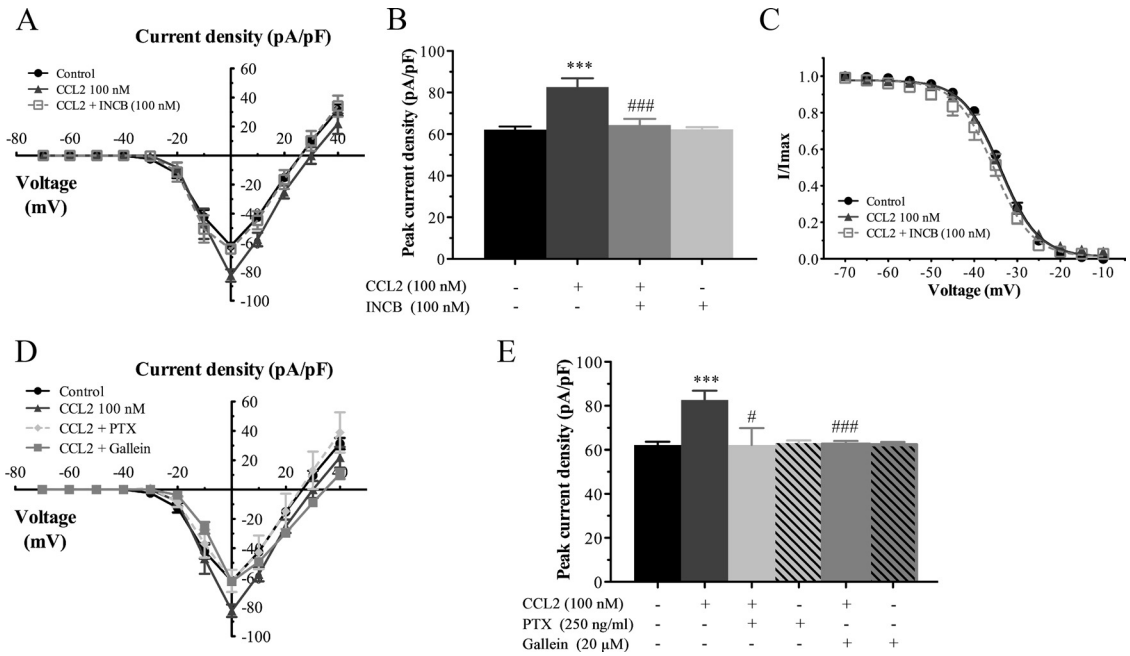

Figure 8. Density and kinetic properties of $Na_v1.8$ currents in medium-sized sensory neurons. ***A***, ***B***, CCL2 increases the maximal peak current amplitude of $Na_v1.8$ ($^{***}p < 0.001$, CCL2 alone vs control). The activation of $Na_v1.8$ currents induced by CCL2 is inhibited after treatment with INCB3344 ($^{###}p < 0.001$ compared with CCL2 alone; Student's *t* test). ***C***, No change in the steady-state inactivation curve of $Na_v1.8$ was seen following CCL2 treatment ($n = 6–11$). ***D***, ***E***, Both PTX and gallein reverse CCL2-induced $Na_v1.8$ current activation ($^{#}p < 0.05$ and $^{###}p < 0.001$ compared with CCL2 alone, respectively). Half-maximal potentials ($V_{1/2}$) and slope (k) values are reported in Table 2. Error bars indicate SEM.

Table 2. Activation and steady-state inactivation characteristics of $Na_v1.8$ currents in medium-sized sensory neurons

	$V_{1/2act}$ (mV)	k_{act}	$V_{1/2inact}$ (mV)	k_{inact}
Control	−6.25 ± 0.44 ($n = 18$)	5.53 ± 0.38	−33.76 ± 0.13 ($n = 11$)	4.19 ± 0.11
CCL2 (100 nM)	−7.76 ± 0.12 ($n = 11$)	4.19 ± 0.10	−34.21 ± 0.26 ($n = 6$)	5.12 ± 0.25
CCL2 (100 nM) + INCB3344 (100 nM)	−9.85 ± 0.15 ($n = 7$)	4.38 ± 0.15	−35.63 ± 0.23 ($n = 7$)	5.17 ± 0.23
CCL2 (100 nM) + PTX (250 ng/ml)	−8.66 ± 0.19 ($n = 5$)	3.62 ± 0.20	ND	ND
CCL2 (100 nM) + gallein (20 μM)	−6.07 ± 0.09 ($n = 11$)	3.72 ± 0.06	ND	ND

$V_{1/2}$ and k determine the half-maximal membrane potential and the slope factor for channel activation and inactivation, respectively. The numbers in parentheses reflect numbers of recorded neurons. ND, Not determined.

CCR2 antagonists represent potential new pain-relieving drugs (Struthers and Pasternak, 2010).

Downstream CCR2 signaling in sensory neurons

Different underlying mechanisms have been proposed to explain how inflammatory mediators acting via GPCR increased $Na_v1.8$ currents and nociceptor excitability (Priest, 2009; Lampert et al., 2010). In particular, the $Na_v1.8$ channel was described as a final common target for several second-messenger cascades, including PKA, PKC, and p38 MAPK (Dib-Hajj et al., 2009b, 2010). As a classical GPCR, CCR2 is functionally coupled to Gα and G$\beta\gamma$ subunits of trimeric G-proteins and activates multiple signal transduction pathways, such as phospholipase C, ERK1/2, and p38 MAPK (Bajetto et al., 2002; Gosselin et al., 2008). Here, we thus investigated the mechanisms that governed the increase of $Na_v1.8$ activity following CCL2 treatment. Our data strongly suggest

that CCL2/CCR2 enhances $Na_v1.8$ currents in a $G_{i/o}$-protein-dependent manner in both small- and medium-sized DRG neurons. Specifically, we showed that preventing $G_{i/o}$ recruitment by PTX treatment completely reversed CCL2-induced inhibition of neuronal cAMP production, potentiation of $Na_v1.8$ current density, as well as the shifts in activation and inactivation kinetics. The full inhibition of $Na_v1.8$ currents by PTX further excludes the involvement of additional G-proteins in the modulation of $Na_v1.8$ by CCL2. Since PTX inhibits the dissociation of $G\beta\gamma$ from $G\alpha i\beta\gamma$ complex (Smrcka et al., 2008), we next examined the participation of $G\beta\gamma$ downstream signaling to CCL2-related $Na_v1.8$ activation. Our results demonstrated that the specific $G\beta\gamma$ dimer inhibitor gallein fully blocked the activation of $Na_v1.8$ currents in response to CCL2 in both populations of sensory neurons. Consequently, these findings suggest that the classical cAMP/PKA signaling pathway resulting from the activation of PTX-sensitive $G_{\alpha i}$ proteins is not involved in the regulation of $Na_v1.8$ by CCL2.

Interestingly, we also found that CCL2 differently influenced the biophysical properties of $Na_v1.8$ in DRG neuron subpopulations. In small sensory neurons, CCL2 increased $Na_v1.8$ current amplitude, which was associated with hyperpolarizing shifts in voltage dependence of both activation and inactivation curves. In contrast, treatment of medium-sized DRG cells with CCL2 only affected the $Na_v1.8$ current density without altering the gating properties of the channel. The different actions of CCL2 may thus reflect the implication of distinct signaling pathways. Based on previous findings (Gold et al., 1998; Vijayaragavan et al., 2004), we might speculate that, in small sensory neurons, CCL2 increases $Na_v1.8$ current density and produces changes in voltage dependence of activation and inactivation via PKC phosphorylation of serine residues within the I–II loop of the $Na_v1.8$ α subunit. Above all, we might propose that the stimulation of PLCβ via the release of $G\beta\gamma$-dimers mediates the activation of PKCε, a PKC isoform shown to potentiate $Na_v1.8$ current (Smrcka, 2008; Cang et al., 2009). In contrast, we might hypothesize that CCL2 regulates $Na_v1.8$ function in medium-sized DRG neurons via a p38 MAPK-dependent pathway (Jin and Gereau, 2006; Hudmon et al., 2008), the activities of p38 MAPK being stimulated by mechanisms that involve dissociation of $\beta\gamma$ subunits (Goldsmith and Dhanasekaran, 2007). Alternatively, as for N-type Ca^{2+} channels and inwardly rectifying K^+ channels (Smrcka, 2008), direct binding of free $G\beta\gamma$ subunits to the C-terminal domain of sodium channel may induce persistent Na^+ currents in neurons (Ma et al., 1997; Mantegazza et al., 2005).

Given the important role played by CCL2 in neuronal–glial interactions and in the temporal onset of pathological pain, we identified here a new mechanism by which CCL2 probably promotes peripheral sensitization and pain hypersensitivity. Since hyperexcitability and spontaneous action potential firing mediated by $Na_v1.8$ in sensory neurons are thought to be the source of some types of chronic pain states, inhibition of CCL2/CCR2 signaling represents a promising avenue for therapeutic intervention.

References

Abbadie C, Lindia JA, Cumiskey AM, Peterson LB, Mudgett JS, Bayne EK, DeMartino JA, MacIntyre DE, Forrest MJ (2003) Impaired neuropathic pain responses in mice lacking the chemokine receptor CCR2. Proc Natl Acad Sci U S A 100:7947–7952.

Amir R, Argoff CE, Bennett GJ, Cummins TR, Durieux ME, Gerner P, Gold MS, Porreca F, Strichartz GR (2006) The role of sodium channels in chronic inflammatory and neuropathic pain. J Pain 7:S1–S29.

Bajetto A, Bonavia R, Barbero S, Schettini G (2002) Characterization of chemokines and their receptors in the central nervous system: physiopathological implications. J Neurochem 82:1311–1329.

Bear B, Asgian J, Termin A, Zimmermann N (2009) Small molecules targeting sodium and calcium channels for neuropathic pain. Curr Opin Drug Discov Devel 12:543–561.

Bhangoo S, Ren D, Miller RJ, Henry KJ, Lineswala J, Hamdouchi C, Li B, Monahan PE, Chan DM, Ripsch MS, White FA (2007) Delayed functional expression of neuronal chemokine receptors following focal nerve demyelination in the rat: a mechanism for the development of chronic sensitization of peripheral nociceptors. Mol Pain 3:38.

Bhangoo SK, Ripsch MS, Buchanan DJ, Miller RJ, White FA (2009) Increased chemokine signaling in a model of HIV1-associated peripheral neuropathy. Mol Pain 5:48.

Bhattacharya A, Wickenden AD, Chaplan SR (2009) Sodium channel blockers for the treatment of neuropathic pain. Neurotherapeutics 6:663–678.

Brodmerkel CM, Huber R, Covington M, Diamond S, Hall L, Collins R, Leffet L, Gallagher K, Feldman P, Collier P, Stow M, Gu X, Baribaud F, Shin N, Thomas B, Burn T, Hollis G, Yeleswaram S, Solomon K, Friedman S, et al. (2005) Discovery and pharmacological characterization of a novel rodent-active CCR2 antagonist, INCB3344. J Immunol 175:5370–5378.

Cang CL, Zhang H, Zhang YQ, Zhao ZQ (2009) PKCepsilon-dependent potentiation of TTX-resistant Nav1.8 current by neurokinin-1 receptor activation in rat dorsal root ganglion neurons. Mol Pain 5:33.

Cummins TR, Waxman SG (1997) Downregulation of tetrodotoxin-resistant sodium currents and upregulation of a rapidly repriming tetrodotoxin-sensitive sodium current in small spinal sensory neurons after nerve injury. J Neurosci 17:3503–3514.

Cummins TR, Sheets PL, Waxman SG (2007) The roles of sodium channels in nociception: implications for mechanisms of pain. Pain 131:243–257.

Dansereau MA, Gosselin RD, Pohl M, Pommier B, Mechighel P, Mauborgne A, Rostene W, Kitabgi P, Beaudet N, Sarret P, Melik-Parsadaniantz S (2008) Spinal CCL2 pronociceptive action is no longer effective in CCR2 receptor antagonist-treated rats. J Neurochem 106:757–769.

Devor M (2006) Sodium channels and mechanisms of neuropathic pain. J Pain 7:S3–S12.

Dib-Hajj SD, Binshtok AM, Cummins TR, Jarvis MF, Samad T, Zimmermann K (2009a) Voltage-gated sodium channels in pain states: role in pathophysiology and targets for treatment. Brain Res Rev 60:65–83.

Dib-Hajj SD, Black JA, Waxman SG (2009b) Voltage-gated sodium channels: therapeutic targets for pain. Pain Med 10:1260–1269.

Dib-Hajj SD, Cummins TR, Black JA, Waxman SG (2010) Sodium channels in normal and pathological pain. Annu Rev Neurosci 33:325–347.

Docherty RJ, Farmer CE (2009) The pharmacology of voltage-gated sodium channels in sensory neurones. Handb Exp Pharmacol 2009:519–561.

Dworkin RH, O'Connor AB, Audette J, Baron R, Gourlay GK, Haanpää ML, Kent JL, Krane EJ, Lebel AA, Levy RM, Mackey SC, Mayer J, Miaskowski C, Raja SN, Rice AS, Schmader KE, Stacey B, Stanos S, Treede RD, Turk DC, et al. (2010) Recommendations for the pharmacological management of neuropathic pain: an overview and literature update. Mayo Clin Proc 85:S3–S14.

Ebersberger A, Natura G, Eitner A, Halbhuber KJ, Rost R, Schaible HG (2011) Effects of prostaglandin D_2 on tetrodotoxin-resistant Na^+ currents in DRG neurons of adult rat. Pain 152:1114–1126.

England S (2008) Voltage-gated sodium channels: the search for subtype-selective analgesics. Expert Opin Investig Drugs 17:1849–1864.

Gao YJ, Ji RR (2010) Chemokines, neuronal-glial interactions, and central processing of neuropathic pain. Pharmacol Ther 126:56–68.

Gao YJ, Zhang L, Samad OA, Suter MR, Yasuhiko K, Xu ZZ, Park JY, Lind AL, Ma Q, Ji RR (2009) JNK-induced MCP-1 production in spinal cord astrocytes contributes to central sensitization and neuropathic pain. J Neurosci 29:4096–4108.

Gold MS, Reichling DB, Shuster MJ, Levine JD (1996) Hyperalgesic agents increase a tetrodotoxin-resistant Na^+ current in nociceptors. Proc Natl Acad Sci U S A 93:1108–1112.

Gold MS, Levine JD, Correa AM (1998) Modulation of TTX-R INa by PKC and PKA and their role in PGE2-induced sensitization of rat sensory neurons *in vitro*. J Neurosci 18:10345–10355.

Goldsmith ZG, Dhanasekaran DN (2007) G protein regulation of MAPK networks. Oncogene 26:3122–3142.

Gosselin RD, Varela C, Banisadr G, Mechighel P, Rostene W, Kitabgi P, Melik-Parsadaniantz S (2005) Constitutive expression of CCR2 chemokine receptor and inhibition by MCP-1/CCL2 of GABA-induced currents in spinal cord neurones. J Neurochem 95:1023–1034.

Gosselin RD, Dansereau MA, Pohl M, Kitabgi P, Beaudet N, Sarret P, Mélik

Parsadaniantz S (2008) Chemokine network in the nervous system: a new target for pain relief. Curr Med Chem 15:2866–2875.

Hudmon A, Choi JS, Tyrrell L, Black JA, Rush AM, Waxman SG, Dib-Hajj SD (2008) Phosphorylation of sodium channel $Na_v1.8$ by p38 mitogen-activated protein kinase increases current density in dorsal root ganglion neurons. J Neurosci 28:3190–3201.

Irannejad R, Wedegaertner PB (2010) Regulation of constitutive cargo transport from the *trans*-Golgi network to plasma membrane by Golgi-localized G protein betagamma subunits. J Biol Chem 285:32393–32404.

Jin X, Gereau RW 4th (2006) Acute p38-mediated modulation of tetrodotoxin-resistant sodium channels in mouse sensory neurons by tumor necrosis factor-α. J Neurosci 26:246–255.

Jung H, Toth PT, White FA, Miller RJ (2008) Monocyte chemoattractant protein-1 functions as a neuromodulator in dorsal root ganglia neurons. J Neurochem 104:254–263.

Jung H, Bhangoo S, Banisadr G, Freitag C, Ren D, White FA, Miller RJ (2009) Visualization of chemokine receptor activation in transgenic mice reveals peripheral activation of CCR2 receptors in states of neuropathic pain. J Neurosci 29:8051–8062.

Lai J, Porreca F, Hunter JC, Gold MS (2004) Voltage-gated sodium channels and hyperalgesia. Annu Rev Pharmacol Toxicol 44:371–397.

Lampert A, O'Reilly AO, Reeh P, Leffler A (2010) Sodium channelopathies and pain. Pflugers Arch 460:249–263.

Lehmann DM, Seneviratne AM, Smrcka AV (2008) Small molecule disruption of G protein beta gamma subunit signaling inhibits neutrophil chemotaxis and inflammation. Mol Pharmacol 73:410–418.

Liu C, Li Q, Su Y, Bao L (2010) Prostaglandin E2 promotes Na1.8 trafficking via its intracellular RRR motif through the protein kinase A pathway. Traffic 11:405–417.

Ma JY, Catterall WA, Scheuer T (1997) Persistent sodium currents through brain sodium channels induced by G protein betagamma subunits. Neuron 19:443–452.

Mantegazza M, Yu FH, Powell AJ, Clare JJ, Catterall WA, Scheuer T (2005) Molecular determinants for modulation of persistent sodium current by G-protein $\beta\gamma$ subunits. J Neurosci 25:3341–3349.

Matulenko MA, Scanio MJ, Kort ME (2009) Voltage-gated sodium channel blockers for the treatment of chronic pain. Curr Top Med Chem 9:362–376.

MeLean MJ, Bennett PB, Thomas RM (1988) Subtypes of dorsal root ganglion neurons based on different inward currents as measured by whole-cell voltage clamp. Mol Cell Biochem 80:95–107.

Menetski J, Mistry S, Lu M, Mudgett JS, Ransohoff RM, Demartino JA, Macintyre DE, Abbadie C (2007) Mice overexpressing chemokine ligand 2 (CCL2) in astrocytes display enhanced nociceptive responses. Neuroscience 149:706–714.

Miller RJ, Jung H, Bhangoo SK, White FA (2009) Cytokine and chemokine regulation of sensory neuron function. Handb Exp Pharmacol 2009:417–449.

Oh SB, Tran PB, Gillard SE, Hurley RW, Hammond DL, Miller RJ (2001) Chemokines and glycoprotein120 produce pain hypersensitivity by directly exciting primary nociceptive neurons. J Neurosci 21:5027–5035.

Priest BT (2009) Future potential and status of selective sodium channel blockers for the treatment of pain. Curr Opin Drug Discov Devel 12:682–692.

Rittner HL, Brack A (2006) Chemokines and pain. Curr Opin Investig Drugs 7:643–646.

Rostène W, Kitabgi P, Parsadaniantz SM (2007) Chemokines: a new class of neuromodulator? Nat Rev Neurosci 8:895–903.

Rostène W, Dansereau MA, Godefroy D, Van Steenwinckel J, Reaux-Le Goazigo A, Mélik-Parsadaniantz S, Apartis E, Hunot S, Beaudet N, Sarret P (2011) Neurochemokines: a menage a trois providing new insights on the functions of chemokines in the central nervous system. J Neurochem 118:680–694.

Roy ML, Narahashi T (1992) Differential properties of tetrodotoxin-sensitive and tetrodotoxin-resistant sodium channels in rat dorsal root ganglion neurons. J Neurosci 12:2104–2111.

Rush AM, Waxman SG (2004) PGE2 increases the tetrodotoxin-resistant Nav1.9 sodium current in mouse DRG neurons via G-proteins. Brain Res 1023:264–271.

Rush AM, Craner MJ, Kageyama T, Dib-Hajj SD, Waxman SG, Ranscht B (2005) Contactin regulates the current density and axonal expression of tetrodotoxin-resistant but not tetrodotoxin-sensitive sodium channels in DRG neurons. Eur J Neurosci 22:39–49.

Serrano A, Paré M, McIntosh F, Elmes SJ, Martino G, Jomphe C, Lessard E, Lembo PM, Vaillancourt F, Perkins MN, Cao CQ (2010) Blocking spinal CCR2 with AZ889 reversed hyperalgesia in a model of neuropathic pain. Mol Pain 6:90.

Smrcka AV (2008) G protein betagamma subunits: central mediators of G protein-coupled receptor signaling. Cell Mol Life Sci 65:2191–2214.

Smrcka AV, Lehmann DM, Dessal AL (2008) G protein betagamma subunits as targets for small molecule therapeutic development. Comb Chem High Throughput Screen 11:382–395.

Struthers M, Pasternak A (2010) CCR2 antagonists. Curr Top Med Chem 10:1278–1298.

Sun JH, Yang B, Donnelly DF, Ma C, LaMotte RH (2006) MCP-1 enhances excitability of nociceptive neurons in chronically compressed dorsal root ganglia. J Neurophysiol 96:2189–2199.

Swanwick RS, Pristerá A, Okuse K (2010) The trafficking of $Na_V1.8$. Neurosci Lett 486:78–83.

Tanaka T, Minami M, Nakagawa T, Satoh M (2004) Enhanced production of monocyte chemoattractant protein-1 in the dorsal root ganglia in a rat model of neuropathic pain: possible involvement in the development of neuropathic pain. Neurosci Res 48:463–469.

Ukhanov K, Brunert D, Corey EA, Ache BW (2011) Phosphoinositide 3-kinase-dependent antagonism in mammalian olfactory receptor neurons. J Neurosci 31:273–280.

Van Steenwinckel J, Reaux-Le Goazigo A, Pommier B, Mauborgne A, Dansereau MA, Kitabgi P, Sarret P, Pohl M, Mélik Parsadaniantz S (2011) CCL2 released from neuronal synaptic vesicles in the spinal cord is a major mediator of local inflammation and pain after peripheral nerve injury. J Neurosci 31:5865–5875.

Vijayaragavan K, Boutjdir M, Chahine M (2004) Modulation of Nav1.7 and Nav1.8 peripheral nerve sodium channels by protein kinase A and protein kinase C. J Neurophysiol 91:1556–1569.

Wang JG, Strong JA, Xie W, Yang RH, Coyle DE, Wick DM, Dorsey ED, Zhang JM (2008) The chemokine CXCL1/growth related oncogene increases sodium currents and neuronal excitability in small diameter sensory neurons. Mol Pain 4:38.

White FA, Miller RJ (2010) Insights into the regulation of chemokine receptors by molecular signaling pathways: functional roles in neuropathic pain. Brain Behav Immun 24:859–865.

White FA, Sun J, Waters SM, Ma C, Ren D, Ripsch M, Steflik J, Cortright DN, Lamotte RH, Miller RJ (2005) Excitatory monocyte chemoattractant protein-1 signaling is up-regulated in sensory neurons after chronic compression of the dorsal root ganglion. Proc Natl Acad Sci U S A 102:14092–14097.

White FA, Feldman P, Miller RJ (2009) Chemokine signaling and the management of neuropathic pain. Mol Interv 9:188–195.

Zhang J, Shi XQ, Echeverry S, Mogil JS, De Koninck Y, Rivest S (2007) Expression of CCR2 in both resident and bone marrow-derived microglia plays a critical role in neuropathic pain. J Neurosci 27:12396–12406.

Zhou Y, Li GD, Zhao ZQ (2003) State-dependent phosphorylation of epsilon-isozyme of protein kinase C in adult rat dorsal root ganglia after inflammation and nerve injury. J Neurochem 85:571–580.